Efficient Transverse Stress Calculation and Failure Prediction in arbitrarily curved Shell-Structures Using TRAVEST

Philipp G. Nolden*, Raimund Rolfes and Guido Kuhlmann

German Aerospace Center - Institute of Structural Mechanics

Lilienthalplatz 7 - 38110 Braunschweig - Germany

Abstract

The transverse components of the stress tensor are highly relevant for failure of composite structures. The extended 2D-method provides a very efficient postprocessing tool for calculating accurate thickness distributions of the transverse stresses from the results of a two-dimensional analysis.

A formulation of this technique for application to arbitrarily curved shell-structures has been developed. In combination with modern failure criteria, it has been implemented into the software-package TRAVEST for postprocessing results from MSC.Nastran.

*Corresponding author (Telephone: ++49[0]531-295-2295 - eMail: Philipp.Nolden@dlr.de)

1 Introduction

Due to their high weight saving potential, modern fibre composite structures more and more replace conventional metallic components, even in primary structural elements like wing and fuselage. In contrast to nearly isotropic materials, the transverse components of the stress tensor are critical for structural failure. Thus, the very poor precision of transverse stresses from two-dimensional analyses is not sufficient for the design process of composite structures.

On the other hand, three–dimensional computation is not suitable for design processes, due to it's high numerical effort. Thus, new computational tools are required, which fulfill both requirements, high numerical efficiency and high precision of the thickness-distributions of the transverse stress components.

Several techniques for structural analysis with regard to the transverse stress distributions have been developed. These include three-dimensional and quasi three-dimensional elements as well as two–dimensional elements based on higher order shear deformation theories - either laminatewise nonlinear or layerwise approximations. Another approach are postprocessing-techniques based on conventional FE–calculations with classical shell-elements based on the first order shear deformation theory (FSDT).

The extended 2D-method by *Rohwer* and *Rolfes* uses the equilibrium conditions which yield very precise thickness distributions of the transverse stresses. By expressing the strain components by the stress resultants, neglecting the influence of the membrane normal force derivatives and eventually assuming cylindrical bending, the transverse stress components are expressed by the transverse shear forces and their first derivatives, respectively. Since the transverse shear forces depend on the deflections and their first derivatives, sufficient results for the transverse stresses can be obtained from second order approximation functions for the displacements. With other words, the transverse stress analysis can be based on a conventional two–dimensional FEA with parabolic elements.

Theory and numerical results for plates have been presented in [8] as well as in [9] and [10]. Results for plates and cylindrical shells are shown in [11]. Now the theory has been extended to arbitrarily curved shells. The derived equations have been implemented into the software package TRAVEST to be used as a postprocessor for results from two-dimensional computations with MSC.Nastran. Since TRAVEST has been integrated into the MSC.Patran toolbox, usage is rather easy and comfortable. In the following section the theory of the current version will be described. Later, the user-interface will be presented and some numerical examples will illustrate the capability of this technique.

2 Theory

The assumptions of the extended 2D-method are mentioned in [8].

2.0.1 The Coordinate System

Since the cartesian coordinates can not directly be used as surface coordinates for curved shells, a curvilinear coordinate system has to be introduced. Here coordinates based on *Huang* and *Tauchert* [7] with two constantly curved coordinates in the main directions and the third coordinate normal on the mid-surface are used. The radii of curvature of the middle surface are denoted by r_α. The difference between the two curvature radii is $r_d = r_2 - r_1$. r denotes the distance between a specific point and the origin of the inertial coordinate system. In contrast to *Huang* and *Tauchert* the angles and the radius are not directly used as coordinates, but local surface coordinates are introduced (see Figure 1).

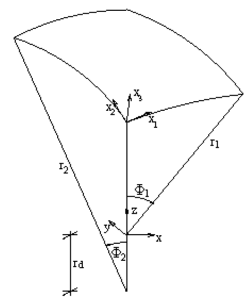

Figure 1: The coordinate system is based on [7] and has constantly curved axes in the shell's main curvature direction.

The surface coordinates are

$$\begin{aligned} x_1 &= \Phi_1 r_1 && (1)\\ x_2 &= \Phi_2 (r_1 + r_d) && (2)\\ x_3 &= r - r_1 && (3) \end{aligned}$$

and the global cartesian coordinates are

$$\begin{aligned} x &= (x_3 + r_1)\sin\frac{x_1}{r_1} && (4)\\ y &= \left[(x_3 + r_1)\cos\frac{x_1}{r_1} + r_d\right]\sin\frac{x_2}{r_2} && (5)\\ z &= \left[(x_3 + r_1)\cos\frac{x_1}{r_1} + r_d\right]\cos\frac{x_2}{r_2}. && (6) \end{aligned}$$

From the covariant basis vectors

$$\begin{aligned} \vec{g}_1 &= \begin{pmatrix} \frac{r}{r_1}\cos\Phi_1 \\ -\frac{r}{r_1}\sin\Phi_1\sin\Phi_2 \\ -\frac{r}{r_1}\sin\Phi_1\cos\Phi_2 \end{pmatrix} && (7)\\ \vec{g}_2 &= \begin{pmatrix} 0 \\ \frac{1}{r_2}\left[r\cos\Phi_1 + r_d\right]\cos\Phi_2 \\ -\frac{1}{r_2}\left[r\cos\Phi_1 + r_d\right]\sin\Phi_2 \end{pmatrix} && (8)\\ \vec{g}_3 &= \begin{pmatrix} \sin\Phi_1 \\ \cos\Phi_1\sin\Phi_2 \\ \cos\Phi_1\cos\Phi_2 \end{pmatrix} && (9) \end{aligned}$$

the covariant metric coefficients

$$g_{11} = \left\{\frac{r}{r_1}\right\}^2 = \left\{\frac{x_3 + r_1}{r_1}\right\}^2 \qquad (10)$$

$$g_{22} = \left\{ \frac{x_3 + r_1}{r_2} \cos\Phi_1 + \frac{r_d}{r_2} \right\}^2 \tag{11}$$

$$g_{33} = 1 \tag{12}$$

$$g_{12} = g_{13} = g_{23} = 0 \tag{13}$$

are derived. Since shallow shells are assumed, the curvature angle Φ_1 is small. Thus, $cos\Phi_1 = 1$. Therefore, the scale factors $h_i = \sqrt{g_{ii}}$ become

$$\begin{array}{ccc} h_1 = \lambda_1; & h_2 = \lambda_2; & h_3 = 1 \\ h_{1,3} = \kappa_1 & h_{2,3} = \kappa_2 & \end{array} \tag{14}$$

with

$$\kappa_\alpha := \frac{1}{r_\alpha} \quad \text{and} \quad \lambda_\alpha := 1 + \frac{x_3}{r_\alpha} = 1 + \kappa_\alpha x_3.$$

2.1 Governing Equations

2.1.1 Strain-Displacement Relationships

The strain-displacement relationships for general coordinates

$$\varepsilon_{ij} = \frac{1}{2}\left[\frac{h_i}{h_j}\left(\frac{u_i}{h_i}\right)_{,j} + \frac{h_j}{h_i}\left(\frac{u_j}{h_j}\right)_{,i} + 2\delta_{ij}\sum_{k=1}^{3}\frac{u_k}{h_i h_k}h_{i,k}\right] \tag{15}$$

are given in [4]. The scale factors for the given coordinates (14) are introduced into (15):

$$\begin{aligned}
\varepsilon_{11} &= \frac{1}{\lambda_1}u_{1,1} + \frac{\kappa_1}{\lambda_1}u_3 \quad ; \quad \varepsilon_{12} = \frac{1}{2}\left[\frac{1}{\lambda_2}u_{1,2} + \frac{1}{\lambda_1}u_{2,1}\right] \\
\varepsilon_{22} &= \frac{1}{\lambda_2}u_{2,2} + \frac{\kappa_2}{\lambda_2}u_3 \quad ; \quad \varepsilon_{13} = \frac{1}{2}\left[u_{1,3} - \frac{\kappa_1}{\lambda_1}u_1 - \frac{1}{\lambda_1}u_{3,1}\right] \\
\varepsilon_{33} &= u_{3,3} \quad ; \quad \varepsilon_{23} = \frac{1}{2}\left[u_{2,3} - \frac{\kappa_2}{\lambda_2}u_2 + \frac{1}{\lambda_2}u_{3,2}\right].
\end{aligned} \tag{16}$$

The kinematic assumptions of Mindlin and Reisner (see e. g. [10]) are introduced into (16). The shell is assumed to be thin with respect to the curve radius: $\lambda_\alpha \to 1$. Therefore, the strain–displacement relationships are

$$\begin{aligned}
\begin{pmatrix} \varepsilon_{11} \\ \varepsilon_{22} \\ \gamma_{12} \end{pmatrix} &= \begin{pmatrix} u^0_{1,1} + \kappa_1 u^0_3 \\ u^0_{2,2} + \kappa_2 u^0_3 \\ u^0_{1,2} + u^0_{2,1} \end{pmatrix} + x_3 \begin{pmatrix} \Theta_{2,1} \\ \Theta_{1,2} \\ \Theta_{2,2} + \Theta_{1,1} \end{pmatrix} \\
\begin{pmatrix} \gamma_{13} \\ \gamma_{23} \end{pmatrix} &= \begin{pmatrix} u^0_{3,1} - \kappa_1 u^0_1 + \Theta_2 \\ u^0_{3,2} - \kappa_2 u^0_2 + \Theta_1 \end{pmatrix} - x_3 \begin{pmatrix} \kappa_1\Theta_2 \\ \kappa_2\Theta_1 \end{pmatrix}.
\end{aligned} \tag{17}$$

2.1.2 Material behaviour

Hooke's law is not different from the plate-theory [8]:

$$\sigma = \mathbf{Q}\left(\epsilon_0 + x_3\kappa\right). \tag{18}$$

2.1.3 Equilibrium Conditions

The equilibrium conditions for general coordinates given in [4] (without external loads)

$$\sum_{j=1}^{3}\left\{\frac{h_1 h_2 h_3 h_i \cdot \sigma_{ij}}{h_j}\right\}_{,j} - \sum_{j=1}^{3}\frac{h_1 h_2 h_3 h_{j,i} \cdot \sigma_{jj}}{h_j} = 0 \tag{19}$$

become for the given coordinates

$$\frac{1}{\lambda_1}\sigma_{11,1} + \frac{1}{\lambda_2}\sigma_{12,2} + \sigma_{13,3} + \left[2\frac{\kappa_1}{\lambda_1} + \frac{\kappa_2}{\lambda_2}\right]\sigma_{13} = 0 \tag{20}$$

$$\frac{1}{\lambda_1}\sigma_{21,1} + \frac{1}{\lambda_2}\sigma_{22,2} + \left[\frac{\kappa_1}{\lambda_1} + 2\frac{\kappa_2}{\lambda_2}\right]\sigma_{23} + \sigma_{23,3} = 0 \tag{21}$$

$$\frac{1}{\lambda_1}\sigma_{31,1} + \frac{1}{\lambda_2}\sigma_{32,2} + \left[\frac{\kappa_1}{\lambda_1} + \frac{\kappa_2}{\lambda_2}\right]\sigma_{33} + \sigma_{33,3} - \frac{\kappa_1}{\lambda_1}\sigma_{11} - \frac{\kappa_2}{\lambda_2}\sigma_{22} = 0. \tag{22}$$

2.2 Transverse Shear Stress Calculation

Integration by parts of the first two equilibrium conditions (20) and (21) yields an equation system for the transverse shear stress components:

$$\tau_3 = \begin{pmatrix} \tau_{13} \\ \tau_{23} \end{pmatrix} = -\mathbf{\Lambda}\int_{\zeta=0}^{\zeta=x_3}\left(\mathbf{B}_1\sigma_{,1} + \mathbf{B}_2\sigma_{,2}\right)d\zeta \tag{23}$$

with

$$\mathbf{B}_1 = \begin{pmatrix} \lambda_1\lambda_2 & 0 & 0 \\ 0 & 0 & \lambda_2^2 \end{pmatrix}; \quad \mathbf{B}_2 = \begin{pmatrix} 0 & 0 & \lambda_1^2 \\ 0 & \lambda_1\lambda_2 & 0 \end{pmatrix}; \quad \mathbf{\Lambda} = \begin{pmatrix} \frac{1}{\lambda_1^2\lambda_2} & 0 \\ 0 & \frac{1}{\lambda_1\lambda_2^2} \end{pmatrix}.$$

This system contains the first derivatives of the membrane stress components with respect to the membrane coordinates. Since the membrane stresses depend on the first derivatives of the displacement vector, the second derivatives of the degrees of freedom are required. In order to reduce the degree of derivation by one, the transverse shear stress components are to be expressed by the transverse shear forces. The first step to achieve this goal is to express the strains by the stress resultants after having introduced Hooke's law (18) into (23). Afterwards the influence of the membrane normal force derivatives will be neglected and cylindrical bending will be assumed. These three steps together yield the reduction of the required degree of derivation.

2.2.1 Expressing the strain through the stress resultants

The elasticity law of the laminate

$$\begin{aligned} \mathbf{N} &= \mathbf{A}\cdot\varepsilon^0 + \mathbf{B}\cdot\kappa \qquad (24)\\ \mathbf{M} &= \mathbf{B}\cdot\varepsilon^0 + \mathbf{D}\cdot\kappa \qquad (25)\end{aligned}$$

is solved for the strain components:

$$\begin{aligned} \varepsilon^0 &= \tilde{\mathbf{A}}^*\cdot\mathbf{N} - \tilde{\mathbf{B}}^*\cdot\mathbf{M} \qquad (26)\\ \kappa &= -\tilde{\mathbf{B}}^*\cdot\mathbf{N} + \tilde{\mathbf{D}}^*\cdot\mathbf{M} \qquad (27)\end{aligned}$$

with

$$\begin{aligned} \tilde{\mathbf{A}}^* &= \mathbf{A}^{-1} + \mathbf{A}^{-1}\mathbf{B}\tilde{\mathbf{D}}^*\mathbf{B}\mathbf{A}^{-1}\\ \tilde{\mathbf{B}}^* &= \tilde{\mathbf{D}}^*\mathbf{B}\mathbf{A}^{-1}\\ \tilde{\mathbf{D}}^* &= \left(\mathbf{D} - \mathbf{B}^T\mathbf{A}^{-1}\mathbf{B}\right)^{-1}.\end{aligned}$$

2.2.2 Calculating the Transverse Shear Stresses from the Transverse Shear Forces

First (18) and then (26) and (27) are introduced into (23):

$$\begin{aligned}\tau_3 = -\Lambda\int_{\zeta=0}^{\zeta=x_3} &\Big\{\mathbf{B}_1\mathbf{Q}\left[\left(\tilde{\mathbf{A}}^*\mathbf{N}_{,1} - \tilde{\mathbf{B}}^*\mathbf{M}_{,1}\right) + \zeta\left(-\tilde{\mathbf{B}}^*\mathbf{N}_{,1} + \tilde{\mathbf{D}}^*\mathbf{M}_{,1}\right)\right]\\ &+ \mathbf{B}_2\mathbf{Q}\left[\left(\tilde{\mathbf{A}}^*\mathbf{N}_{,2} - \tilde{\mathbf{B}}^*\mathbf{M}_{,2}\right) + \zeta\left(-\tilde{\mathbf{B}}^*\mathbf{N}_{,2} + \tilde{\mathbf{D}}^*\mathbf{M}_{,2}\right)\right]\Big\}\,d\zeta.\end{aligned} \qquad (28)$$

Expression (28) is integrated analytically:

$$\begin{aligned}\tau_3 = -\Lambda\Bigg\{&\begin{bmatrix}\mathbf{A}_1 & \mathbf{0}\\ \mathbf{0} & \mathbf{A}_3\end{bmatrix}\left(\begin{bmatrix}\mathbf{a}_{12}\tilde{\mathbf{A}}^* - \mathbf{b}_{12}\tilde{\mathbf{B}}^*\\ \mathbf{a}_{22}\tilde{\mathbf{A}}^* - \mathbf{b}_{22}\tilde{\mathbf{B}}^*\end{bmatrix}\mathbf{N}_{,1} + \begin{bmatrix}-\mathbf{a}_{12}\tilde{\mathbf{B}}^* + \mathbf{b}_{12}\tilde{\mathbf{D}}^*\\ -\mathbf{a}_{22}\tilde{\mathbf{B}}^* + \mathbf{b}_{22}\tilde{\mathbf{D}}^*\end{bmatrix}\mathbf{M}_{,1}\right)\\ +&\begin{bmatrix}\mathbf{A}_3 & \mathbf{0}\\ \mathbf{0} & \mathbf{A}_2\end{bmatrix}\left(\begin{bmatrix}\mathbf{a}_{11}\tilde{\mathbf{A}}^* - \mathbf{b}_{11}\tilde{\mathbf{B}}^*\\ \mathbf{a}_{12}\tilde{\mathbf{A}}^* - \mathbf{b}_{12}\tilde{\mathbf{B}}^*\end{bmatrix}\mathbf{N}_{,2} + \begin{bmatrix}-\mathbf{a}_{11}\tilde{\mathbf{B}}^* + \mathbf{b}_{11}\tilde{\mathbf{D}}^*\\ -\mathbf{a}_{12}\tilde{\mathbf{B}}^* + \mathbf{b}_{12}\tilde{\mathbf{D}}^*\end{bmatrix}\mathbf{M}_{,2}\right)\Bigg\}\end{aligned} \qquad (29)$$

with the boolean vectors

$$\mathbf{A}_1 = \begin{bmatrix}1 & 0 & 0\end{bmatrix};\quad \mathbf{A}_2 = \begin{bmatrix}0 & 1 & 0\end{bmatrix};\quad \mathbf{A}_3 = \begin{bmatrix}0 & 0 & 1\end{bmatrix}$$

and the partial stiffnesses

$$\mathbf{a}_{\alpha\beta}(x_3) = \int_{\zeta=0}^{\zeta=x_3}\lambda_\alpha\lambda_\beta\mathbf{Q}\,d\zeta = \mathbf{z}_0(x_3) + (\kappa_\alpha + \kappa_\beta)\,\mathbf{z}_1(x_3) + \kappa_\alpha\kappa_\beta\mathbf{z}_2(x_3) \qquad (30)$$

and

$$\mathbf{b}_{\alpha\beta}(x_3) \;=\; \int_{\zeta=0}^{\zeta=x_3} \lambda_\alpha \lambda_\beta \mathbf{Q} \zeta d\zeta \;=\; \mathbf{z}_1(x_3) + (\kappa_\alpha + \kappa_\beta)\,\mathbf{z}_2(x_3) + \kappa_\alpha \kappa_\beta \mathbf{z}_3(x_3) \tag{31}$$

where

$$\begin{aligned} \mathbf{z}_i(x_3) &= \int_{\zeta=0}^{\zeta=x_3} \zeta^i \mathbf{Q} d\zeta = \int_{\zeta=x_3^{(k)}}^{\zeta=x_3} \zeta^i \mathbf{Q}^{(k)} d\zeta + \sum_{j=1}^{k-1} \int_{x_3^{(j)}}^{x_3^{(j+1)}} \zeta^i \mathbf{Q}^{(j)} d\zeta \\ &= \frac{1}{i+1} \mathbf{Q}^{(k)} \left(x_3^{i+1} - x_{3k}^{i+1} \right) + \frac{1}{i+1} \sum_{j=1}^{k-1} \mathbf{Q}^{(j)} \left(x_{3j+1}^{i+1} - x_{3j}^{i+1} \right). \end{aligned} \tag{32}$$

Now some abbrevations are introduced:

$$\mathbf{F}_{\alpha\beta} \;=\; \mathbf{a}_{\alpha\beta} \tilde{\mathbf{B}}^* - \mathbf{b}_{\alpha\beta} \tilde{\mathbf{D}}^* \tag{33}$$

$$\mathbf{G}_{\alpha\beta} \;=\; -\mathbf{a}_{\alpha\beta} \tilde{\mathbf{A}}^* + \mathbf{b}_{\alpha\beta} \tilde{\mathbf{B}}^* \tag{34}$$

and

$$\begin{aligned} \mathbf{A}_k \mathbf{G}_{\alpha\beta} &\rightarrow \mathbf{G}_{\alpha\beta}^k \\ \mathbf{A}_k \mathbf{F}_{\alpha\beta} &\rightarrow \mathbf{F}_{\alpha\beta}^k. \end{aligned}$$

The influence of the membrane normal force derivatives is neglected and cylindrical bending is assumed:

$$\mathbf{M}_{,1} = \begin{pmatrix} R_{13} \\ 0 \\ 0 \end{pmatrix}; \quad \mathbf{M}_{,2} = \begin{pmatrix} 0 \\ R_{23} \\ 0 \end{pmatrix}.$$

$R_{\alpha 3}$ denote the transverse shear forces.

Another abbrevation is introduced

$$\mathbf{F}_{\alpha\beta}^k \mathbf{A}_\gamma^T \rightarrow \mathbf{F}_{\alpha\beta}^{k\gamma}$$

and eventually a simple relation between the transverse shear stresses and the transverse shear forces can be specified:

$$\tau_3 = \Lambda \begin{bmatrix} \mathbf{F}_{12}^{11} & \mathbf{F}_{11}^{32} \\ \mathbf{F}_{22}^{31} & \mathbf{F}_{12}^{22} \end{bmatrix} \begin{bmatrix} R_{13} \\ R_{23} \end{bmatrix}. \tag{35}$$

2.2.3 Computation of the Transverse Shear Forces

The forces can be calculated using the material law

$$\mathbf{R} = \mathbf{H}\gamma, \tag{36}$$

where $\mathbf{H}$ is the matrix of transverse shear stiffnesses. The vector of transverse shear strains γ can be calculated from the nodal degrees of freedom $\mathbf{u}$ and the shape functions and their first derivatives comprised in the matrix $\mathbf{B}_s$:

$$\gamma = \mathbf{B}_s \mathbf{u} \tag{37}$$

(see [9]).

Using equations (35), (36) and (37) the transverse shear stresses can be computed with only first derivatives of the shape funktions, in contrast to the more obvious way using (23), (18) and (17) which would require second derivatives.

2.3 Transverse Normal Stress

The third equilibrium condition (22), by using integration by parts, can be transformed into a condition for the transverse normal stress:

$$\sigma_{33} = -\frac{1}{\lambda_1\lambda_2}\int \left\{\lambda_2\tau_{13,1} + \lambda_1\tau_{23,2} - \kappa_1\lambda_2\sigma_{11} - \kappa_2\lambda_1\sigma_{22}\right\} dx_3 + \frac{c_3}{\lambda_1\lambda_2}. \tag{38}$$

The FSDT leads to linear membrane normal strains through the thickness and the stiffnesses are layerwise constant. Thus, the membrane normal stresses are layerwise linear:

$$\sigma_{\alpha\alpha}^{(k)} = \sigma_{\alpha\alpha}^{B(k)} + \frac{\sigma_{\alpha\alpha}^{T(k)} - \sigma_{\alpha\alpha}^{B(k)}}{x_3^{(k+1)} - x_3^{(k)}}\left(x_3 - x_3^{(k)}\right). \tag{39}$$

The formerly derived condition for the transverse shear stresses (35) is introduced, and thus the condition for the transverse normal stress is

$$\begin{aligned}
\sigma_{33} \;=\; & -\frac{1}{\lambda_1\lambda_2}\left\{\left[\int_{x_3^{(1)}}^{x_3}\frac{1}{\lambda_1^2}\mathbf{a}_{12}d\zeta\cdot\tilde{\mathbf{B}}^* - \int_{x_3^{(1)}}^{x_3}\frac{1}{\lambda_1^2}\mathbf{b}_{12}d\zeta\cdot\tilde{\mathbf{D}}^*\right]^{11} R_{13,1}\right.\\
& + \left[\int_{x_3^{(1)}}^{x_3}\frac{1}{\lambda_1^2}\mathbf{a}_{11}d\zeta\cdot\tilde{\mathbf{B}}^* - \int_{x_3^{(1)}}^{x_3}\frac{1}{\lambda_1^2}\mathbf{b}_{11}d\zeta\cdot\tilde{\mathbf{D}}^*\right]^{32} R_{23,1}\\
& + \left[\int_{x_3^{(1)}}^{x_3}\frac{1}{\lambda_2^2}\mathbf{a}_{22}d\zeta\cdot\tilde{\mathbf{B}}^* - \int_{x_3^{(1)}}^{x_3}\frac{1}{\lambda_2^2}\mathbf{b}_{22}d\zeta\cdot\tilde{\mathbf{D}}^*\right]^{31} R_{13,2}\\
& + \left[\int_{x_3^{(1)}}^{x_3}\frac{1}{\lambda_2^2}\mathbf{a}_{12}d\zeta\cdot\tilde{\mathbf{B}}^* - \int_{x_3^{(1)}}^{x_3}\frac{1}{\lambda_2^2}\mathbf{b}_{12}d\zeta\cdot\tilde{\mathbf{D}}^*\right]^{22} R_{23,2}\\
& - \sum_{\alpha=1}^{2}\left\{\kappa_\alpha\lambda_\beta\left[\sigma_{\alpha\alpha}^{B(k)}\left(x_3 - x_3^{(k)}\right) - \frac{1}{2}\frac{\sigma_{\alpha\alpha}^{T(k)} - \sigma_{\alpha\alpha}^{B(k)}}{x_3^{(k+1)} - x_3^{(k)}}\left(x_3 - x_3^{(k)}\right)^2\right.\right.\\
& \qquad\qquad \left. + \frac{\sigma_{\alpha\alpha}^{T(k)} - \sigma_{\alpha\alpha}^{B(k)}}{x_3^{(k+1)} - x_3^{(k)}}x_3^{(k)}\left(x_3 - x_3^{(k)}\right)\right]\\
& + \sum_{j=1}^{k-1}\kappa_\alpha\lambda_\beta\left[\sigma_{\alpha\alpha}^{B(j)}\left(x_3^{(j+1)} - x_3^{(j)}\right) - \frac{1}{2}\frac{\sigma_{\alpha\alpha}^{T(j)} - \sigma_{\alpha\alpha}^{B(j)}}{x_3^{(j+1)} - x_3^{(j)}}\left(x_3^{(j+1)} - x_3^{(j)}\right)^2\right.\\
& \qquad\qquad \left.\left.\left. + \frac{\sigma_{\alpha\alpha}^{T(j)} - \sigma_{\alpha\alpha}^{B(j)}}{x_3^{(j+1)} - x_3^{(j)}}x_3^{(j)}\left(x_3^{(j+1)} - x_3^{(j)}\right)\right]\right\}\right\}
\end{aligned} \tag{40}$$

with

$$\int_{x_3^{(1)}}^{x_3}\frac{1}{\lambda_\alpha^2}\mathbf{a}_{\alpha\beta}d\zeta \;=\; \frac{1}{\lambda_\alpha}\left[\frac{1}{2}\left(x_3 - x_3^{(k)}\right)^2 + \frac{\kappa_\beta}{6}\left(x_3 - x_3^{(k)}\right)^2\left(x_3 + 2x_3^{(k)}\right)\right]\mathbf{Q}^{(k)}$$

$$
\begin{aligned}
&+\sum_{l=1}^{k-1}\frac{1}{\lambda_\alpha^{(l+1)}}\left[\frac{1}{2}\left(x_3^{(l+1)}-x_3^{(l)}\right)^2\right.\\
&\qquad\left.+\frac{\kappa_\beta}{6}\left(x_3^{(l+1)}-x_3^{(l)}\right)^2\left(x_3^{(l+1)}+2x_3^{(l)}\right)\right]\mathbf{Q}^{(l)}\\
&+\frac{1}{\lambda_\alpha^{(l)}}\frac{1}{\lambda_\alpha^{(k)}}\left(x_3-x_3^{(k)}\right)\mathbf{a}_{\alpha\beta}(x_3^{(k)})\\
&+\sum_{l=1}^{k-1}\frac{1}{\lambda_\alpha^{(l+1)}}\frac{1}{\lambda_\alpha^{(l)}}\left(x_3^{(l+1)}-x_3^{(l)}\right)\mathbf{a}_{\alpha\beta}(x_3^{(l)})
\end{aligned}
\tag{41}
$$

and

$$
\begin{aligned}
\int_{x_3^{(k)}}^{x_3}\frac{1}{\lambda_\alpha^2}\mathbf{b}_{\alpha\beta}d\zeta \;=\;& \frac{\left(x_3-x_3^{(k)}\right)^2}{6\lambda_\alpha}\left[\left(x_3+2x_3^{(k)}\right)+\frac{\kappa_\beta}{2}\left(x_3^2+2x_3x_3^{(k)}+3x_3^{(k)2}\right)\right]\mathbf{Q}^{(k)}\\
&+\sum_{l=1}^{k-1}\left\{\frac{\left(x_3^{(l+1)}-x_3^{(l)}\right)^2}{6\lambda_\alpha^{(l+1)}}\left[\left(x_3^{(l+1)}+2x_3^{(l)}\right)\right.\right.\\
&\qquad\left.\left.+\frac{\kappa_\beta}{2}\left(x_3^{(l+1)2}+2x_3^{(l+1)}x_3^{(l)}+3x_3^{(l)2}\right)\right]\;\mathbf{Q}^{(l)}\right\}\\
&+\frac{1}{\lambda_\alpha}\frac{1}{\lambda_\alpha^{(k)}}\left(x_3-x_3^{(k)}\right)\mathbf{b}_{\alpha\beta}(x_3^{(k)})\\
&+\sum_{l=1}^{k-1}\frac{1}{\lambda_\alpha^{(l+1)}}\frac{1}{\lambda_\alpha^{(l)}}\left(x_3^{(l+1)}-x_3^{(l)}\right)\mathbf{b}_{\alpha\beta}(x_3^{(l)})
\end{aligned}
\tag{42}
$$

and $\alpha \neq \beta$. The transverse shear force derivatives can be computed using (36) and (37). Since in (37) only the shape functions and their derivatives depend on the membrane coordinates, the transverse shear force derivatives are

$$\mathbf{R}_{,\alpha} = \mathbf{H}\mathbf{B}_{s,\alpha}\mathbf{u}. \tag{43}$$

Since $\mathbf{B}_s$ contains the shape functions and their first derivatives, the computation of the transverse normal stresses requires the second derivatives of the shape functions. The traditional alternative using (38), (18) and (17) would require the third derivative. For a complete failure analysis considering all transverse stress components, only second order instead of third order shape functions are needed in the deformation analysis. With other words, we can use QUAD8-elements in conjunction with TRAVEST.

2.4 Failure Criteria

By providing an accurate and physically feasible three-dimensional state of stress, TRAVEST offers the possibility to carry out a complete failure analysis with physically well founded three-dimensional failure criteria. Currently five different criteria for unidirectional composite layers under three-dimensional stress are implemented:

1. TSai-Wu criterion (TSW)

2. Criterion of **HAS**hin (HAS)
3. Invariant Approach of Cuntze (IAC)
4. Parabolic Criterion of Puck (PCP) and
5. the Simple Parabolic Criterion (SPC).

All these are macromechanical and stress-based criteria which have the form

$$F(f_R(\sigma) \cdot \sigma) = 1 \tag{44}$$

wherein $f_R(\sigma)$ is the so called reserve factor (see [5] as well as [1], [2], [3], [6] and [13] for details). Failure occurs for $F(f_R(\sigma) \cdot \sigma) \geq 1$.

HAS, IAC, PCP and SPC support the determination of a failure mode which denotes the critical component by a boolean value. "1" signifies fibre fracture (FF) and "2" stands for inter fibre fracture (IFF).

3 Implementation

The transverse shear forces and their derivatives - see (36), (37) and (43) - depend only on the nodal degrees of freedom of the current element. Therefore, the transverse stress analysis with the extended 2D-method can be carried out element-wise.

Since the method requires second derivatives, at least parabolic shape functions are needed. Currently TRAVEST can be applied on QUAD8 and TRIA6 elements. Additional options for postprocessing results from linear and bilinear elements like the far more popular QUAD4 element are challenges for future developement.

The curvature of the undeformed structure within the element is assumed to have constant radii, defined by the three node positions on each element edge, in both directions. Thus, the formerly developed equations are valid.

TRAVEST reads the nodal translations and rotations from the MSC.Nastran database and applies the formerly described procedure of stress analysis on these results. The consequential stress tensor can further be used for an advanced failure analysis. Details about the failure analysis options will be discussed in future publications.

4 User Interface

4.1 TRAVEST in the Design Process

The extended 2D-method itself has the main advantage to be a pure postprocessing tool for the analysis of results from any two-dimensional deformation analysis using the FSDT. It is suitable for analytic solution as well as for any kind of Finite Element solution, subject to the condition that the shape functions are at least parabolic.

Primary interest lies of course on the application to FE-analyses with the smallest possible degree of shape functions. Therefore the current available version of TRAVEST can postprocess results from QUAD8 and TRIA6 MSC.Nastran elements.

Since being a pure postprocessing tool, the extended 2D-method can easily be integrated into the industrial design process. If the designer decides to use a composite material for his structure, the computational

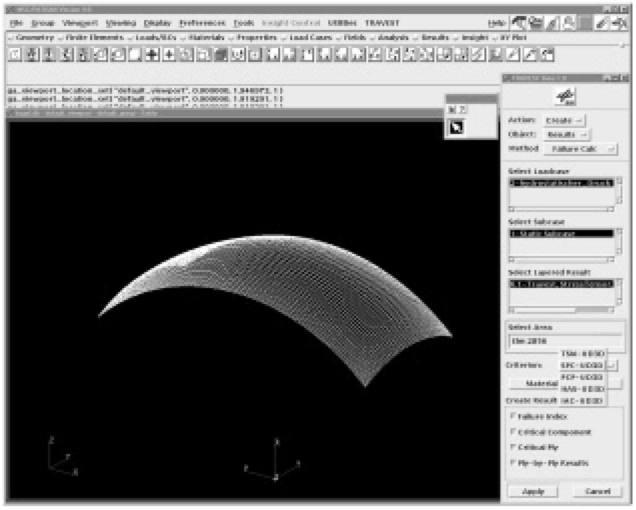

Figure 2: TRAVEST provides user-friendly options for transverse stress analysis and failure analysis. This figure shows the screenshot of a MSC.Patran session while choosing the desired failure criterion in the TRAVEST form.

engineer only has to add a rather small additional calculation with TRAVEST requiring a much smaller numerical cost than the two-dimensional FE-calculation itself to fulfill the higher demands of the failure analysis. So TRAVEST allows to make the step to much more sophisticated structures without fundamental changes in the design process.

This illustrates one of the the main advantages over other approaches for calculating the thickness distributions of the transverse stress components: The today well-known and widely-used FE-tools do not have to be modified or even replaced. Tools and numerical effort nearly stay the same from analysis of metallic structures except one relatively small additional program which carries out an additional calculation with small numerical cost compared to the FE-deformation-analysis. The FE-analysis itself has in principle no difference from the FE-analysis of the complementary metallic structure at all.

4.2 Using TRAVEST with MSC.Patran

In order to minimize the effort of integrating TRAVEST into the familiar design process, it has been integrated into the MSC.Patran toolbox. To perform a complete failure analysis considering the complete three-dimensional stress tensor, the user has to carry out a traditional FE-deformation analysis using MSC.Nastran first. When the results are available, the particular steps to the complete failure prediction are the following:

First the input form has to be opened by activating the TRAVEST-button in the MSC.Patran main menu. The user can choose between transverse stress analysis and failure calculation.

The input form depends on, if the user has chosen the transverse stress calculation or failure calculation (see figure 3). In any case, the area, in which the analysis is to be carried out, now has to be chosen. This can

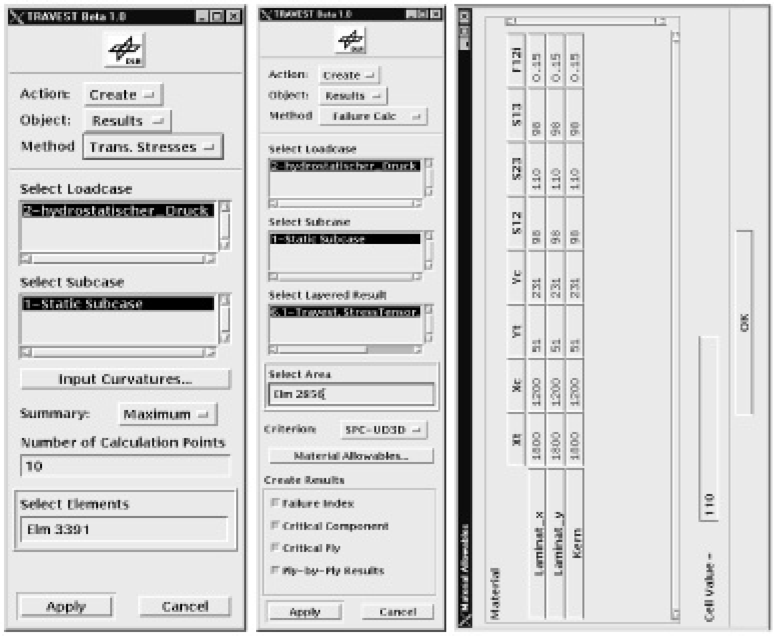

Figure 3: The TRAVEST form for stress analysis (left), failure calculation (middle) and the form for the material allowables (right)

be done by editing the "Select Elements" and the "Select Area" option, respectively, or simply by mouseclick in the viewport.

If the transverse stress analysis option has been chosen, the number of calculation points over the thickness has to be chosen and the analysis can be started after having activated the desired loadcase and subcase. The computed transverse shear and normal stresses are stored in the .trav_stress-file and the database and can easily be visualized with MSC.Patran or any other suitable data analysis software, for example *gnuplot*.

If a complete failure prediction is desired, the user can choose between several different failure criteria. Further the material allowables have to be defined (figure 3, right). The default values are realistic for typical carbon fibre reinforced plastics, but the result of the failure analysis of course strongly depends on the specific strength parameters of the chosen material. Thus, the user has to care for reliable material parameters to provide reliable results.

Last but not least, the user has to specify in the "create results"-field (see figure 3, middle), which result parameters he is especially interested in.

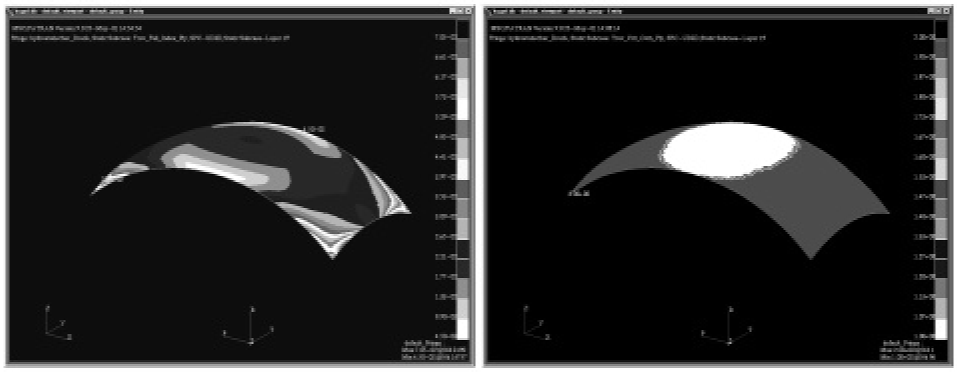

Figure 4: The material effort (left) and the failure mode (right) can be visualised as contour plot in the MSC.Patran viewport (here for the lowest layer). The failure mode is a boolean value that identifies the critical component. In the red area it is likely, that the matrix would fail. In the white area, the fibre would rather fail.

All failure prediction results can comfortably be visualized with the MSC.Patran viewport, choosing the "results" option. Examples of contour plots of the failure index and the failure mode are shown in figure 4 (left) and figure 4 (right), respectively.

5 Numerical Examples

TRAVEST stress results are presented for a spherical shell with curvature radii $r_\alpha = 1.0$ and a saddle shell with $[r_1 = -2.0; r_2 = 1.0]$ (see figure (5)). Both consist of a three-layered [0/90/0]-composite with thickness $t = \frac{r_2}{20} = 0.5 \quad \hat{=} \quad [0.01\bar{6}]_3$. The material parameters are given in table 1. On each structure, a bisinusodial

E_1	=	181.1	G_{12}	=	7.71
E_2	=	10.3	G_{23}	=	2.39
ν_{12}	=	0.28	G_{13}	=	7.71

Table 1: Material parameters for the example structures

pressure with a maximum of 1.0 in the center and 0.0 around the edges is applied (50% as positive pressure on the top surface and 50% as negative pressure on the sub surface) and on all edges, radial translations are fixed.

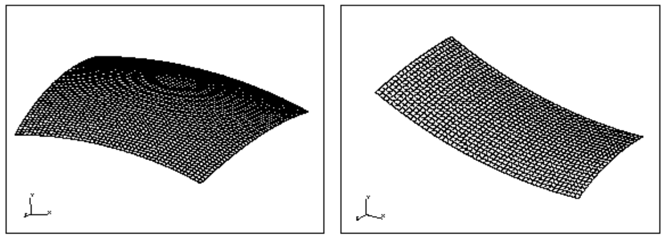

Figure 5: The prediction capabilities of TRAVEST are demonstrated with two example models, a spherical shell (left) and a saddle shell (right).

Since spheres and saddle shells have constant curvature radii in the main directions, they can be described within a curvilinear coordinate system $\vec{r} = (\Phi_1, \Phi_2, r)$ corresponding to *Huang* and *Tauchert* (see figure 1). The middle surface lies in the plain spanned by the curvilinear coordinates Φ_α. The edges are parallel to the coordinate axes at $\Phi_\alpha = 0.0$ and $\Phi_\alpha = 0.5$.

Reference solutions are derived from three-dimensional FE-ananlyses and - for the spherical structure - from an analytical analysis based on [12].

Figure 6 shows the thickness distributions of two transverse stress components for the spherical shell. The transverse stress components for the saddle shell are shown in figure 7. The plots show a feasible

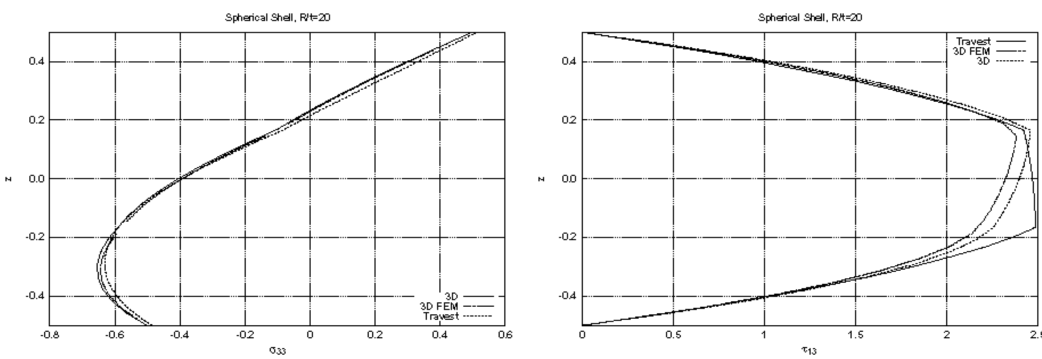

Figure 6: TRAVEST results for a spherical shell structure. The transverse stress components are evaluated at their maxima with respect to the membrane coordinates.

distribution, compared to the three-dimensional solutions, with low deviance. The FSDT would provide a layerwise constant transverse shear stress which would not fulfill the equilibrium conditions. The transverse normal stress would be zero.

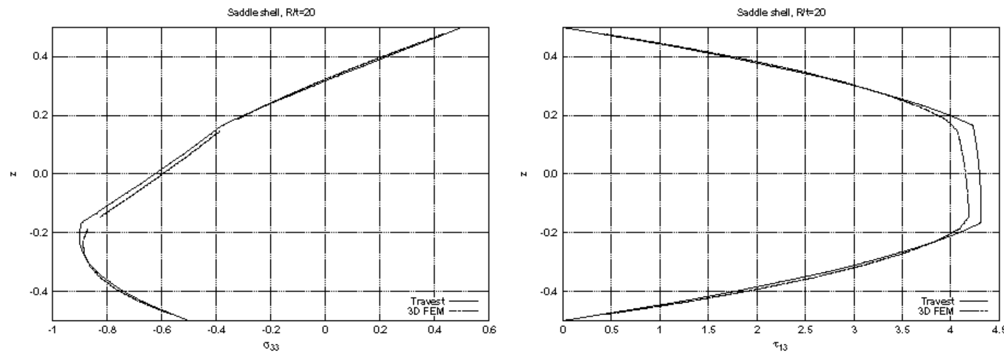

Figure 7: TRAVEST results for a saddle panel. The transverse stress components are again evaluated at their maxima with respect to the membrane coordinates.

6 Conclusion

TRAVEST spares the FE-analyst from carrying out an expensive three–dimensional analysis in the case of examining composite structures. In contrast to other approaches to this demand, the extended 2D-method has the advantage of using the well established two-dimensional FE-tools. Thus, the relatively big step forward from two–dimensional to three-dimensional stress and failure analysis is realised just by integrating an additional software package into the design process, which at least leads to nothing more than some extra mouseclicks for the user.

This paper presents the complete theoretical background for the extended 2D-method for a special class of curvilinear coordinate systems. In FE-analyis, these can be used to describe generally curved structures by assuming elementwise constant radii. Therefore, with this paper all required information for three-dimensional stress analysis in shallow shell structures with the extended 2D-method, can be obtained.

Besides demonstrating the complete theoretical basis for the extended 2D-method in curvilinear space, the main purpose of this article has been to demonstrate the user interface. It has been shown that by integrating TRAVEST into MSC.Patran, it is a perfectly easy step to a complete and precise three-dimensional stress and failure analysis.

7 Acknowledgements

The authors would like to thank the MSC.Software Corporation for several years of fruitful and inspiring cooperation.

References

[1] R. G. Cuntze: "The Failure Mode Concept - a new comprehensive 3D-strength Analysis Concept for any brittle and ductile behaving Material", Proceedings European Conference on Spacecraft Structures, Materials and Mechanical Testing, Braunschweig, 1998.

[2] R. G. Cuntze et al.: "Neue Bruchkriterien und Festigkeitsnachweise für unidirektionale Faserverbundwerkstoffe unter mehrachsiger Beanspruchung - Modellbildung und Experimente", Fortschrittsberichte VDI, Vol. 5 No. 506, VDI Verlag Düsseldorf, 1997.

[3] Z. Hashin: "Failure Criteria for unidirectional Fiber Composites", *Journal of Applied Mechanics*, Vol. 47, pp. 329-334, 1980.

[4] N. N. Huang: "Exact analysis for three-dimensional free vibrations of cross-ply cylindrical and doubly-curved laminates", *Acta Mechanica* 108, pp. 23-34, 1995.

[5] G. Kuhlmann: *TRAVEST - User's Manual*, Course Notes, Exercises, DLR IB 131-2000/16, Braunschweig, 2000.

[6] A. Puck: *Festigkeitsanalyse von Faser-Matrix-Laminaten: Modelle für die Praxis*, Carl Hanser Verlag, München; Wien, 1996.

[7] N. N. Huang, T. R. Tauchert: "Thermal stresses in doubly-curved cross-ply laminates", *International Journal of Solids and Structures*, Vol. 29, No. 8, pp. 991-1000, 1992.

[8] R. Rolfes, A. K. Noor, K. Rohwer: "Efficient Calculation of Transverse Stresses in Composite Plates", Proceedings of the 1997 MSC User´s Conference, 1997.

[9] R. Rolfes, K. Rohwer, M. Ballerstaedt: "Efficient linear transverse normal stress analysis of layered composite plates", *Computers and Structures*, Vol. 68, pp. 643-652, 1998.

[10] R. Rolfes, K. Rohwer: "Improved Transverse Shear Stresses in Composite Finite Elements Based on First Order Shear Deformation Theory", *International Journal for Numerical Methods in Engineering*, Vol. 40, pp. 51-60, 1997.

[11] K. Rohwer, R. Rolfes: "Calculating 3D Stresses in Layered Composite Plates and Shells", *Mechanics of Composite Materials*, Vol. 34, No. 4, pp. 491-500, 1998.

[12] M. Savoia, J. N. Reddy: "Three-Dimensional Thermal Analysis of Laminated Composite Plates", *International Journal of Solids and Structures*, Vol. 32, No. 5, pp. 593-608, 1995.

[13] S. W. Tsai, E. M. Wu: "A general theory of strength for anisotropic materials", *Journal of Composite Materials*, Vol. 5, pp. 58-80, 1971.